Accelerated structure-based design of chemically diverse allosteric modulators of a muscarinic G protein-coupled receptor

Yinglong Miao[a,b,1,2], Dahlia Anne Goldfeld[b], Ee Von Moo[c], Patrick M. Sexton[c], Arthur Christopoulos[c], J. Andrew McCammon[a,b,d,2], and Celine Valant[c,1,2]

[a]Howard Hughes Medical Institute, University of California at San Diego, La Jolla, CA 92093; [b]Department of Pharmacology, University of California at San Diego, La Jolla, CA 92093; [c]Drug Discovery Biology, Monash Institute of Pharmaceutical Sciences, Monash University, Parkville VIC 3052, Australia; and [d]Department of Chemistry and Biochemistry, University of California at San Diego, La Jolla, CA 92093

Contributed by J. Andrew McCammon, July 27, 2016 (sent for review June 24, 2016; reviewed by Richard J. Lewis and Jung-Hsin Lin)

Design of ligands that provide receptor selectivity has emerged as a new paradigm for drug discovery of G protein-coupled receptors, and may, for certain families of receptors, only be achieved via identification of chemically diverse allosteric modulators. Here, the extracellular vestibule of the M_2 muscarinic acetylcholine receptor (mAChR) is targeted for structure-based design of allosteric modulators. Accelerated molecular dynamics (aMD) simulations were performed to construct structural ensembles that account for the receptor flexibility. Compounds obtained from the National Cancer Institute (NCI) were docked to the receptor ensembles. Retrospective docking of known ligands showed that combining aMD simulations with *Glide* induced fit docking (IFD) provided much-improved enrichment factors, compared with the *Glide* virtual screening workflow. *Glide* IFD was thus applied in receptor ensemble docking, and 38 top-ranked NCI compounds were selected for experimental testing. In [^{3}H]*N*-methylscopolamine radioligand dissociation assays, approximately half of the 38 lead compounds altered the radioligand dissociation rate, a hallmark of allosteric behavior. In further competition binding experiments, we identified 12 compounds with affinity of ≤30 μM. With final functional experiments on six selected compounds, we confirmed four of them as new negative allosteric modulators (NAMs) and one as positive allosteric modulator of agonist-mediated response at the M_2 mAChR. Two of the NAMs showed subtype selectivity without significant effect at the M_1 and M_3 mAChRs. This study demonstrates an unprecedented successful structure-based approach to identify chemically diverse and selective GPCR allosteric modulators with outstanding potential for further structure-activity relationship studies.

GPCR | allosteric modulators | ensemble docking | affinity | cooperativity

The largest group of signal-transmitting proteins at the cell surface is the superfamily of G protein-coupled receptors (GPCRs) (1) that account for targets of ∼40% of currently marketed drugs. For decades, the development of ligands in traditional GPCR-based drug discovery has focused on targeting the primary endogenous ligand (orthosteric) binding site of the receptor (2), guiding the development of most classical orthosteric agonists, inverse agonists, and antagonists (3–6). However, modern discovery targeting GPCRs is characterized by an alarmingly high attrition rate (7). Such moderate clinical outcome can partly be attributed to the inability of most ligands to selectively target one receptor among a family of GPCR subtypes. Many receptor subtypes of GPCR families often exhibit a highly conserved orthosteric binding pocket, such that a single ligand can interact with several receptors simultaneously, leading to the activation/inactivation of multiple receptors, sometimes with opposing of their signaling profiles, contributing to off-target side effects (8). One representative case of a GPCR family displaying dramatically low subtype selectivity is the muscarinic acetylcholine receptors (mAChRs), composed of five distinct subtypes, M_1–M_5 mAChRs, that each binds the endogenous ligand, ACh, with similar affinity. These receptors are broadly distributed within both the central and peripheral nervous systems, as well as various peripheral organs (9).

However, GPCRs often exhibit multiple binding cavities in their structures (10, 11). It is thus possible to design and synthesize ligands capable of binding receptors, away from their orthosteric sites, in less conserved allosteric pockets (12). These ligands, called allosteric modulators, can bind to a GPCR concomitantly to the endogenous (orthosteric) ligand, altering its binding affinity and/or cellular-signaling efficacy, ultimately resulting in a modified pharmacological profile of the ligand–receptor complex (3, 13). Combining their modulatory effects with their potential for selective interaction with less conserved binding sites, allosteric modulators represent an alternate therapeutic approach to treat GPCR-related diseases (14, 15). Unfortunately, despite major interest in targeting allosteric sites of GPCRs, the discovery of allosteric modulators of GPCRs has mainly been serendipitous, with a surprising paucity of structure-based approaches. With recent advances in structural biology techniques, a growing number of GPCR structures have been solved, including four members of the mAChR family (16–19), In particular, the M_2 mAChR has been crystallized in both an inactive state bound by the 3-quinuclidinyl-benzilate (QNB) antagonist (16) and an active state bound to the high-affinity

Significance

Chemical diversity has recently risen as key structural feature for the discovery of novel selective drugs of G protein-coupled receptors (GPCRs). However, the traditional drug discovery technique of combinatorial chemistry coupled to high-throughput screening has become less attractive because of its immense financial impact. To address this problem, we implemented a computer-aided drug design approach, using the M_2 muscarinic acetylcholine receptor (mAChR) as a GPCR model, and performed computational enhanced sampling simulations to account for the receptor flexibility. Through iterative molecular docking and experimental testing, half of the 38 computationally selected National Cancer Institute compounds were validated as allosteric modulators of the M_2 mAChR. Our method successfully identified positive and negative allosteric modulators of M_2 mAChR with unprecedented chemical diversity.

Author contributions: Y.M., A.C., J.A.M., and C.V. designed research; Y.M., D.A.G., E.V.M., and C.V. performed research; Y.M., D.A.G., E.V.M., P.M.S., A.C., J.A.M., and C.V. analyzed data; and Y.M., P.M.S., A.C., J.A.M., and C.V. wrote the paper.

Reviewers: R.J.L., The University of Queensland; and J.-H.L., Academia Sinica.

Conflict of interest statement: A patent on "new allosteric modulators of the M2 muscarinic receptor" has been filed based on findings presented in this study.

[1]Y.M. and C.V. contributed equally to this work.

[2]To whom correspondence may be addressed. Email: yimiao@ucsd.edu, jmccammon@ucsd.edu, or celine.valant@monash.edu.

This article contains supporting information online at www.pnas.org/lookup/suppl/doi:10.1073/pnas.1612353113/-/DCSupplemental.

agonist, iperoxo (IXO), and a G-protein mimetic nanobody (18). Furthermore, the M_2 mAChR is also the first and only GPCR that has been cocrystallized with a positive allosteric modulator (PAM), LY-2119620, bound in the extracellular vestibule (18). Although these crystal structures provided enormously important insights into different specific conformational states, as well as atomistic protein–ligand interactions of GPCRs, they nonetheless represent snapshots of the highly dynamic nature of GPCRs (20). To address the above issue, extensive computational simulations have been performed to characterize the structural dynamics of GPCRs (20–33). All-atom molecular dynamics (MD) simulations are capable of exploring large-scale conformational changes during both receptor activation (23) and deactivation (20) by using fast supercomputers. Moreover, long-timescale MD simulations captured ligand binding to GPCRs (29), in particular for several prototypical negative allosteric modulators (NAMs) of the M_2 mAChR (30). In recent studies, we have also successfully depicted the activation of both the M_2 and M_3 mAChRs in accelerated MD (aMD) simulations (31–33).

In the present study, we combined computational aMD simulations and virtual screening with experimental binding and functional assays to identify and validate allosteric modulators of the M_2 mAChR. The discovery of allosteric modulators with chemically novel structures will undoubtedly increase the potential for better receptor subtype selectivity. Based on the hypothesis that incorporation of receptor flexibility is key to effective GPCR drug design (34, 35), we used aMD simulations to construct structural ensembles for molecular docking in the extracellular vestibule of the receptor. Ensemble docking of chemical compounds obtained from the National Cancer Institute (NCI) compound library (36) was performed to identify new potential allosteric modulators. The computationally selected lead compounds were then tested experimentally to investigate their binding and functional properties. We report here a successful structure-based design approach and several chemically diverse allosteric modulators of the M_2 mAChR. An overview of the procedure followed is shown in Fig. 1.

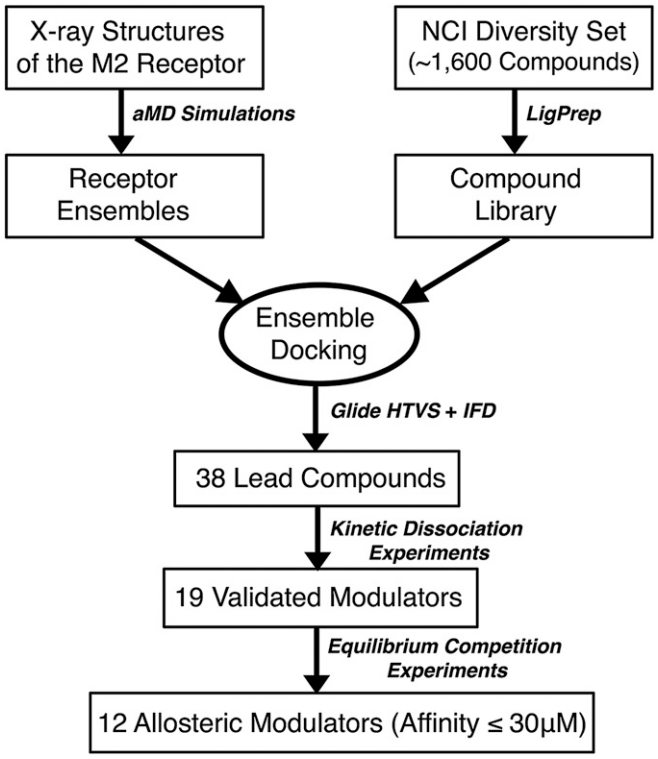

Fig. 1. Overview flowchart for discovering allosteric modulators of the M_2 mAChR. Starting from X-ray structures of the inactive QNB-bound and active IXO-nanobody-bound M_2 receptor, aMD-enhanced sampling simulations were carried out to construct structural ensembles that account for receptor flexibility. Meanwhile, a compound library was prepared from the NCI Diversity Set (~1,600 compounds) by using LigPrep in the Schrödinger package. Ensemble docking was then performed to identify potential allosteric modulators. *Glide* HTVS+IFD was applied and provided much improved enrichment factors in retrospective docking, allowing the selection of 38 top-ranked compounds for experimental testing. Of this set, 19 compounds that significantly slowed the dissociation of the antagonist radioligand [^{3}H]NMS were selected for further characterization. Finally, 12 allosteric modulators exhibited binding affinity of ≤30 μM.

Results

Docking Based on aMD Simulations and *Glide* Virtual Screening Workflow. By using X-ray structures of the inactive QNB-bound and active IXO-nanobody-bound M_2 mAChR, aMD simulations were carried out to construct structural ensembles to account for receptor flexibility (*SI Appendix*, Table S1). Meanwhile, a compound library was prepared from the NCI Diversity Set (~1,600 compounds) by using *LigPrep* in the Schrödinger package. Docking of known orthosteric ligands against the receptor X-ray structures and aMD structural ensembles was first carried out by using Glide virtual screening workflow (VSW) (Schrödinger, LLC). Overall, retrospective docking of the antagonists and agonists using aMD structural ensembles provided significantly higher enrichment factors than using the X-ray structures alone (*SI Appendix*, Tables S3 and S4). Particularly, dihedral aMD ensembles of the active IXO-nanobody-bound receptor led to improved docking, compared with dual-boost aMD ensembles for the inactive QNB-bound receptor. This result is largely because of greater flexibility of the active GPCR state compared with the inactive state (37), and higher acceleration is thus needed for conformational sampling of the latter. In the first round, ensemble docking of the NCI compounds against aMD simulation ensembles of the extracellular allosteric site in the inactive M_2 mAChR was performed to identify potential allosteric modulators. Ten top-ranked compounds were selected for experimental testing using radioligand binding assays. Results showed that one of these compounds, NSC-46385, significantly slowed the dissociation rate of the [^{3}H]*N*-methylscopolamine ([^{3}H]NMS) radioligand (*SI Appendix*, Fig. S3), but with low binding affinity for the M_2 mAChR (≥100 μM) (*SI Appendix*, Table S2). This poor performance was likely because of the fact that the orthosteric site is deeply buried in the receptor, whereas the extracellular allosteric site is exposed on the receptor surface, involving flexible residues such as Trp-422$^{7.35}$ (18, 38).

Docking Based on aMD Simulations and *Glide* Induced Fit Docking. In an effort to optimize our docking protocol and increase the compound success rate, we performed extensive retrospective docking in the second round, using a Glide induced fit docking (IFD) method that scans for different conformations of residue side chains of the protein. Moreover, because IFD calculations are very computationally expensive (~200 CPU hours for every 100 compounds per receptor structure), high-throughput virtual screening (HTVS) was first applied to select the top 100 compounds, which were then subjected to IFD to improve their ranking. Overall, docking of aMD receptor ensembles using the Glide HTVS+IFD provided much improved enrichment factors compared with using the Glide VSW. For the active IXO-nanobody-bound receptor, the Glide HTVS+IFD on aMD structural ensembles provided the greatest enrichment factors when the average binding energy (BE_{avg}) was used for ranking (*SI Appendix*, Table S5). Dihedral aMD simulation was able to sufficiently sample flexible regions on the receptor surface, and in combination with Glide IFD, can fully account for the receptor flexibility for docking. Ensemble docking combining aMD simulation and Glide HTVS+IFD (with BE_{avg} for ranking) was

thus applied to identify allosteric modulators targeting the active IXO-nanobody-bound M_2 receptor. Surprisingly, for the inactive QNB-bound receptor, the Glide HTVS+IFD on the X-ray structure provided the highest enrichment, followed by Glide HTVS+IFD on the dihedral aMD structural ensemble when the minimum binding energy (BE_{min}) was used for ranking (*SI Appendix*, Table S6). Based on this finding, the X-ray and dihedral aMD simulation structures were combined to form the final structural ensemble, and ensemble docking using Glide HTVS+IFD (with BE_{min} for ranking) was adopted for the following virtual screening of the inactive QNB-bound M_2 mAChR.

Compounds Selected Through Optimized Ensemble Docking. A list of 50 top-ranked compounds was obtained from virtual screening of the NCI Diversity Set targeting the active IXO-nanobody-bound M_2 mAChR (*SI Appendix*, Table S7) and another 50 compounds targeting the inactive QNB-bound receptor (*SI Appendix*, Table S8). Among the computationally predicted lead compounds, seven were shared between the two lists (*SI Appendix*, Table S9). Because these seven compounds could have higher probability of binding the M_2 mAChR in both the inactive and active states ("cross hits"), they were selected first for experimental testing. Next, for the active M_2 mAChR, 2 lead compounds that seemed to contain scaffolds of known ligands were selected, along with another 14 compounds that were ranked among the top 20 of the predicted highest-affinity binders. For the inactive M_2 receptor, 3 lead compounds with certain scaffolds of known ligands and 12 compounds that were ranked among the top 20 of the predicted highest-affinity binders were added to the list. Compounds with known scaffolds were used to rationalize our findings, whereas those with chemically diverse and yet-unknown scaffolds could potentially be novel allosteric modulators. In summary, a set of 38 total compounds was collected and ordered from NCI for experimental testing (*SI Appendix*, Table S9). Table 1 lists the top-ranked compounds binding the active and/or inactive M_2 mAChR, for which experimental binding affinities were also determined (more detailed discussion is provided below). For compounds that bind the active receptor, the root-mean-square error (rmse) between experimental and computationally predicted affinities is 2.1 kcal/mol when BE_{avg} obtained from ensemble docking is used for the latter or 4.2 kcal/mol by using BE_{min}. The rmse values for compounds binding to the inactive receptor are 5.0 and 4.7 kcal/mol by using BE_{avg} and BE_{min}, respectively. Notably, significantly higher binding affinities could be obtained by using aMD simulation structures (BE_{min} from ensemble docking) than using the crystal structures. This finding suggests that the receptor conformational change captured through aMD simulation is able to facilitate ligand binding. When only the crystal structures were used for virtual screening, ~50–60% of the experimentally confirmed NCI ligands of the M_2 mAChR could have been missed in this study (Table 1).

Validation of Allosteric Binding at the M_2 mAChR. To investigate the binding mode of our selected ligands, we evaluated their ability to alter the dissociation rate (k_{off}) of the orthosteric antagonist, [^{3}H]NMS. Using a single concentration of putative modulator, 100 μM, we compared the dissociation rates of a K_D concentration (0.1 nM) of [^{3}H]NMS from the orthosteric binding site of the M_2 mAChR, in the absence and presence of NCI compounds (*SI Appendix*, Fig. S4). In the absence of any modulator, at a saturating concentration of atropine to prevent the reassociation of [^{3}H]NMS, the radioligand dissociation rate was estimated at $k_{off} = 0.079 \pm 0.01$ min^{-1} ($n = 2$; mean ± SD). Comparably, in the presence of a concentration of 100 μM of three structurally distinct well-known allosteric modulators, the PAM of [^{3}H]NMS, LY-2033298 (39), and two different NAMs, gallamine and strychnine, all three ligands were able to significantly slow the dissociation rate of [^{3}H]NMS as expected (Fig. 2*A* and *SI Appendix*, Fig. S4*A*). Relative to the control dissociation rate of [^{3}H]NMS, 19 of the 38 selected NCI compounds were significantly slowed by ≥25%, the antagonist dissociation rate, with $k_{off} \leq 0.060$ min^{-1}, and 12 of them with $k_{off} \leq 0.040$ min^{-1} (≥50%) (*SI Appendix*, Fig. S4*B* and Table S10).

Binding Affinity and Cooperativity Estimates of NCI Compounds at the M_2 mAChR. To obtain quantitative information (i.e., binding affinity and cooperativity estimates), we performed two-way interaction binding experiments between a K_D concentration of [^{3}H]NMS and increasing concentrations of each of the selected NCI compounds (*SI Appendix*). For interactions between [^{3}H]NMS and NCI compounds, we used an allosteric ternary complex model for data analysis (3). For each compound that affected the specific binding of [^{3}H]NMS, we could estimate an affinity value, pK_B, for the allosteric site, as well as a binding cooperativity value,

Table 1. Top-ranked NCI compounds that were predicted to bind the active IXO-nanobody-bound and inactive QNB-bound M_2 mAChR

Receptor	NSC ID	BE_{avg} (ensemble)	BE_{min} (ensemble)	BE (crystal)	Rank (crystal)	BE_{exp}
Active (R*)	305798	−9.85	−11.59	−10.27	6	−6.01 ± 0.22
	13316	−9.25	−10.74	−10.36	4	−6.36 ± 0.50
	308814	−9.19	−10.61	n.a.	n.a.	−6.83 ± 0.08
	121868	−8.30	−11.10	n.a.	n.a.	−8.53 ± 0.11
	379697	−8.21	−9.44	n.a.	n.a.	−6.75 ± 0.40
	143491	−8.03	−12.36	−10.80	3	−7.09 ± 0.20
	147866	−7.88	−10.58	n.a.	n.a.	−7.23 ± 0.20
	322661	−6.95	−10.12	−8.92	27	−5.60 ± 0.24
Inactive (R)	143491	−10.06	−12.33	−9.51	23	−7.09 ± 0.20
	371178	−7.72	−12.12	n.a.	n.a.	−6.76 ± 0.28
	322661	−2.01	−11.39	−9.28	29	−5.60 ± 0.24
	305798	−9.54	−11.21	−9.47	26	−6.01 ± 0.22
	121868	−0.74	−10.95	n.a.	n.a.	−8.53 ± 0.11
	13316	−0.61	−10.69	n.a.	n.a.	−6.36 ± 0.50
	99657	−0.66	−10.67	n.a.	n.a.	−7.23 ± 0.27

Units for the binding energies (BE) are kcal/mol. The experimental binding energies were converted from pK_B as $BE = RT \ln K_B$, where R is the gas constant, T is the experimental temperature (310 K), and K_B is the binding equilibrium constant. Based on retrospective docking, compounds binding to the active receptor (R^*) are ranked according to the ensemble-averaged binding energy (BE_{avg}), and those binding to the inactive receptor (R) are ranked according to the minimum binding energy obtained from ensemble docking (BE_{min}). n.a., not applicable.

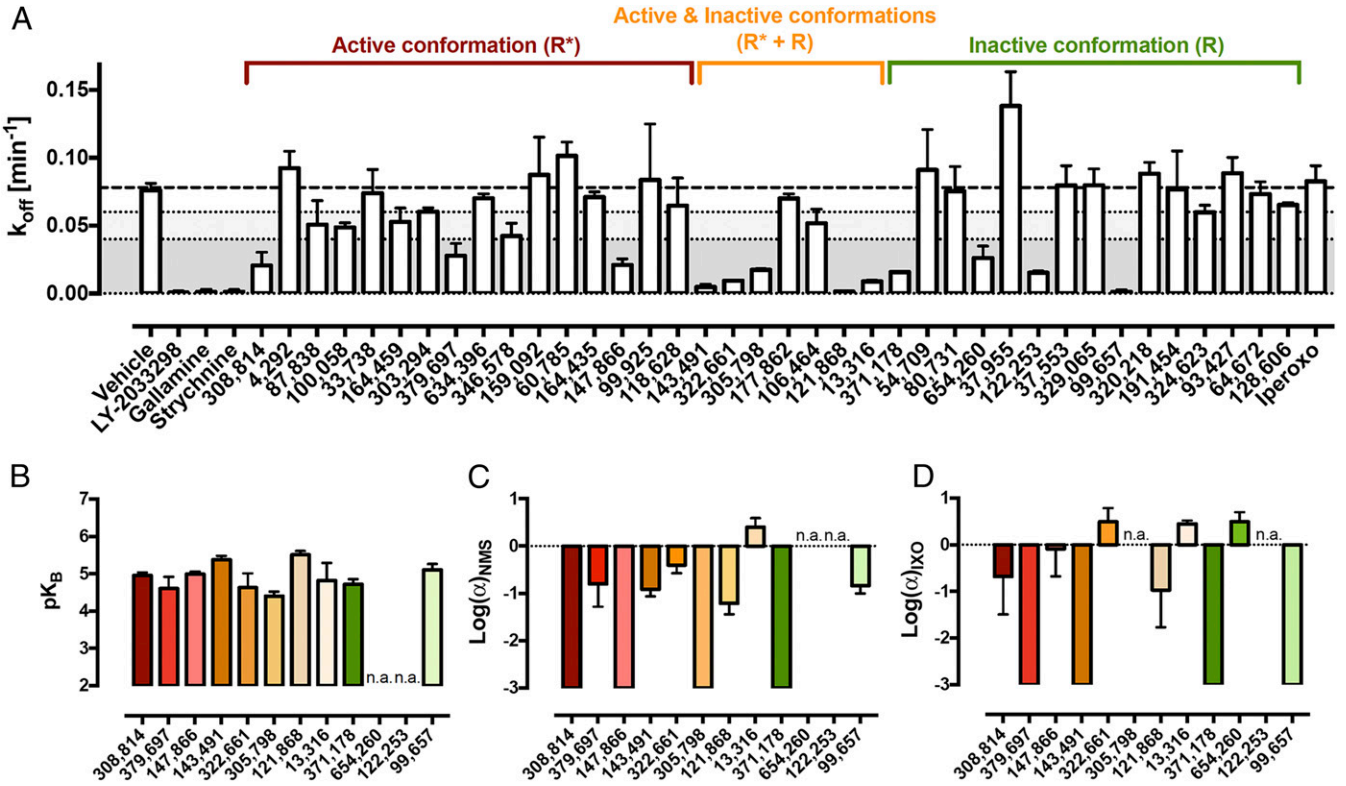

Fig. 2. Allosteric binding properties of NCI compounds at the M_2 mAChR. (*A*) The dissociation rates of the radioligand, [^{3}H]NMS (k_{off}), were revealed by adding 100 μM atropine alone or in the presence of each of the 38 computationally selected lead compounds at a concentration of 100 μM. Included are also the k_{off} values, with three known allosteric modulators (LY-2033298, gallamine, and strychnine) for comparison. Dashed lines show the threshold, $k_{off} \leq 0.06$ min^{-1} (light gray) and $k_{off} \leq 0.04$ min^{-1} (dark gray), that were used to select the 19 or 12 lead compounds for further investigation, respectively. As a negative control, IXO at a concentration of 1 μM (~300 x K_i) was also tested. (*B–D*) Binding affinity (pK_B) of each of the 12 selected NCI compounds (*B*) and cooperativity (Logα) between each NCI compound and [^{3}H]NMS (*C*) and IXO (*D*). n.a., not applicable.

Logα_{NMS}, defining the type of allosteric effect against the radioligand (*SI Appendix*, Fig. S4 *C* and *D*). For the 19 selected NCI compounds that slowed the dissociation rate of [^{3}H]NMS by >25%, 14 of them displayed marked NAM behavior with [^{3}H]NMS; 4 compounds showed neutral cooperativity; and 1 compound exhibited a small, but consistent, PAM effect on radioligand binding (*SI Appendix*, Table S10). Fig. 2 *B* and *C* displays the pK_B and Logα_{NMS} estimates for the 12 NCI compounds that slowed the dissociation rate of [^{3}H]NMS by >50%. Interestingly, two NCI compounds (NSC-654260 and -122253) were classified as neutral allosteric ligands (NALs) because they did not show any alteration of the specific binding of [^{3}H]NMS for the M_2 mAChR, suggesting that although able to slow the dissociation, the affinity (K_D) of the radioligand remained unchanged. This result can be the case for allosteric modulators that also alter the association rate of the radioligand, because $K_D = k_{off}/k_{on}$. Overall, the other 10 NCI compounds altered the binding of [^{3}H]NMS at the M_2 mAChR, with binding affinity for the allosteric site in the range of ~3–30 μM ($4.50 \leq pK_B \leq 5.50$); 9 of the NCI compounds were classified as NAMs, because they displayed significant negative modulation of [^{3}H]NMS binding. Additionally, one NCI compound, NSC-13316, displayed significant PAM activity with the radioligand, Log$\alpha_{NMS} = 0.40 \pm 0.19$. The chemical structures of these 12 compounds are shown in Fig. 3. To quantify the allosteric effect of these NCI compounds on agonist affinity, we performed three-way interaction studies between [^{3}H]NMS and IXO and defined the cooperativity between each of the 12 NCI compounds and the agonist (Fig. 2*D* and *SI Appendix*, Table S10). For the NCI compounds that exhibited high degrees of cooperativity with the radioligand, we performed full interaction curves (i.e., concentration inhibition curve of IXO in the presence of increasing concentrations of modulator). For the two NCI compounds that had no effect on the specific binding of [^{3}H]NMS alone, we performed titration interaction curves (i.e., single fixed concentration of IXO with increasing concentrations of modulators). This latter method is efficient for modulators with limited cooperativity with the orthosteric probe and has the advantage of saving considerable amounts of compounds and time (see *SI Appendix* for more details). Of the 12 NCI compounds investigated, 7 were NAMs of IXO binding with high to medium negative cooperativity ($-3 \leq$ Log$\alpha_{IXO} \leq -0.70$), 2 were NALs and did not affect the affinity of IXO (NSC-305798 and -122253), and 3 appeared to enhance the binding of IXO for the M_2 mAChR (NSC-322661, -13316, and -654260) (Fig. 2*D*).

Distinct Signaling Effects of Novel Allosteric Modulators on Agonist-Mediated Responses. Based on chemical diversities of the 12 NCI lead compounds as shown in Fig. 3 and their specific allosteric properties at the M_2 mAChR, we finally selected 5 compounds (NSC-322661, -121868, -13316, -147866, and -99657), as well as a ligand that appeared to have no effect on binding experiments as a negative control (NSC-93427) to carry on validation of their functional signaling effects (Fig. 4). The effect of each of these six NCI compounds was investigated on the functional response of IXO. The functional assay chosen for this study was phosphorylation of extracellular signal-regulated kinases 1/2 (pERK1/2) because it is downstream of multiple receptor activation pathways and therefore an ideal functional output for detection of small changes in receptor function. We first performed time-course experiments to determine the stimulation period of the

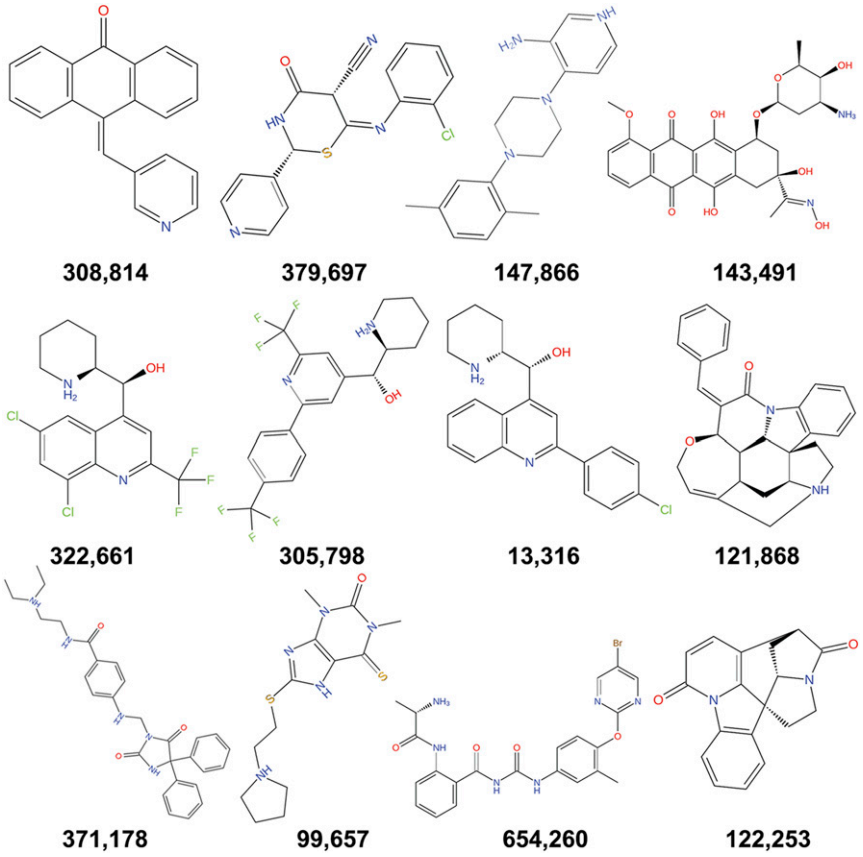

Fig. 3. Chemical structures of the 12 NCI compounds that were validated experimentally as allosteric ligands of the M_2 mAChR. These compounds slowed down the dissociation rates of the [^{3}H]NMS antagonist by ≥50%. In addition, they exhibited significant binding affinities in the range of ∼3–30 μM ($4.50 \leq pK_B \leq 5.50$).

selected NCI compounds, alongside IXO. As expected, IXO showed a robust stimulation of pERK1/2 that peaked at 5 min (*SI Appendix*, Fig. S6*A*). Among the NCI compounds, none appeared to induce the stimulation of pERK1/2 at any time points measured, apart from NSC-322661, which displayed a weak response at ∼7 min. The incubation times of 5 min for IXO and 7 min for NCI compounds were then chosen as the stimulation periods for subsequent functional experiments. To provide estimates of functional cooperativity with IXO ($Log\alpha\beta_{IXO}$), we used the titration format, whereby increasing concentrations of each selected NCI compound were applied to an EC_{70} concentration of IXO, in parallel to a full-concentration response analysis of the agonist alone (Fig. 4 *A*–*F*). Using an allosteric operational model to fit the data, we were able to estimate the compounds' binding affinity (pK_B), as well as functional cooperativity with the agonist, $Log\alpha\beta_{IXO}$. Four NCI compounds, NSC-147866, -121868, -99657, and -13316, significantly reduced the ability of 0.03 nM IXO to induce pERK1/2 ($Log\alpha\beta_{IXO} \sim -3$), indicating strong negative modulation on the agonist-mediated response (Fig. 4 *B*–*D*). Affinities of the four modulators were estimated from our functional assays as pK_B = 5.49 ± 0.34 (NSC-147866), 5.85 ± 0.15 (NSC-121868), 5.46 ± 0.16 (NSC-99657), and 5.21 ± 0.23 (NSC-13316), all strongly agreeing with their respective radioligand equilibrium binding measurements. In contrast, one compound, NSC-322661, showed a small, but consistent, increase of pERK1/2 levels in the presence of 0.03 nM IXO ($Log\alpha\beta_{IXO}$ = 0.74 ± 0.22), suggesting that this compound was a PAM of agonist-mediated response (Fig. 4*A*). As anticipated, NCS-93427 did not show any effect on IXO-mediated pERK1/2 response. Finally, we selected two NCI compounds (NSC-322661 and -13316) to perform full interaction studies between the modulators and IXO (Fig. 4 *G* and *H*). Using an operation model of allosterism constraining the affinity of each modulator (as defined by radioligand binding against [^{3}H]NMS), we defined the functional cooperativity of the two compounds for IXO, $Log\alpha\beta_{IXO}$ equal to approximately –3 for NSC-13316 and $Log\alpha\beta_{IXO}$ = 0.36 ± 0.17 for NSC-322661. For the latter compound, the cooperativity with the agonist was slightly lower than that estimated from the titration method, most likely because of the additional weak partial agonist effect of the compound alone that would affect the basal levels of pERK1/2 at the single concentration of agonist used. Together, these results suggest that our ensemble docking method combining aMD simulations with Glide HTVS+IFD was successfully applied to identify both PAMs and NAMs of the M_2 mAChR. The most favorable binding poses predicted from ensemble docking calculations revealed that NSC-322661 (a PAM of agonist function) is predicted to cause only very small conformational changes in the active IXO-nanobody-bound conformation of the receptor (Fig. 5*A*). In comparison, NSC-13316 (a NAM of agonist function) binds much deeper into the receptor and is predicted to induce larger structural rearrangements of the TM helices (Fig. 5*B*). The largest conformational changes occurred in residues Y426$^{7.39}$, W422$^{7.35}$, Y83$^{2.64}$, and F181 in the extracellular loop (ECL) 2. Therefore, NSC-13316 tends to disrupt the receptor active conformation, which leads to negative allosteric modulation of the M_2 mAChR.

Subtype Selectivity of Modulators on Agonist-Mediated Responses. To assess the potential subtype selectivity of the NCI compounds, we finally investigated their effect on IXO-mediated pERK1/2 responses at the two most peripherally expressed subtypes, M_1 and

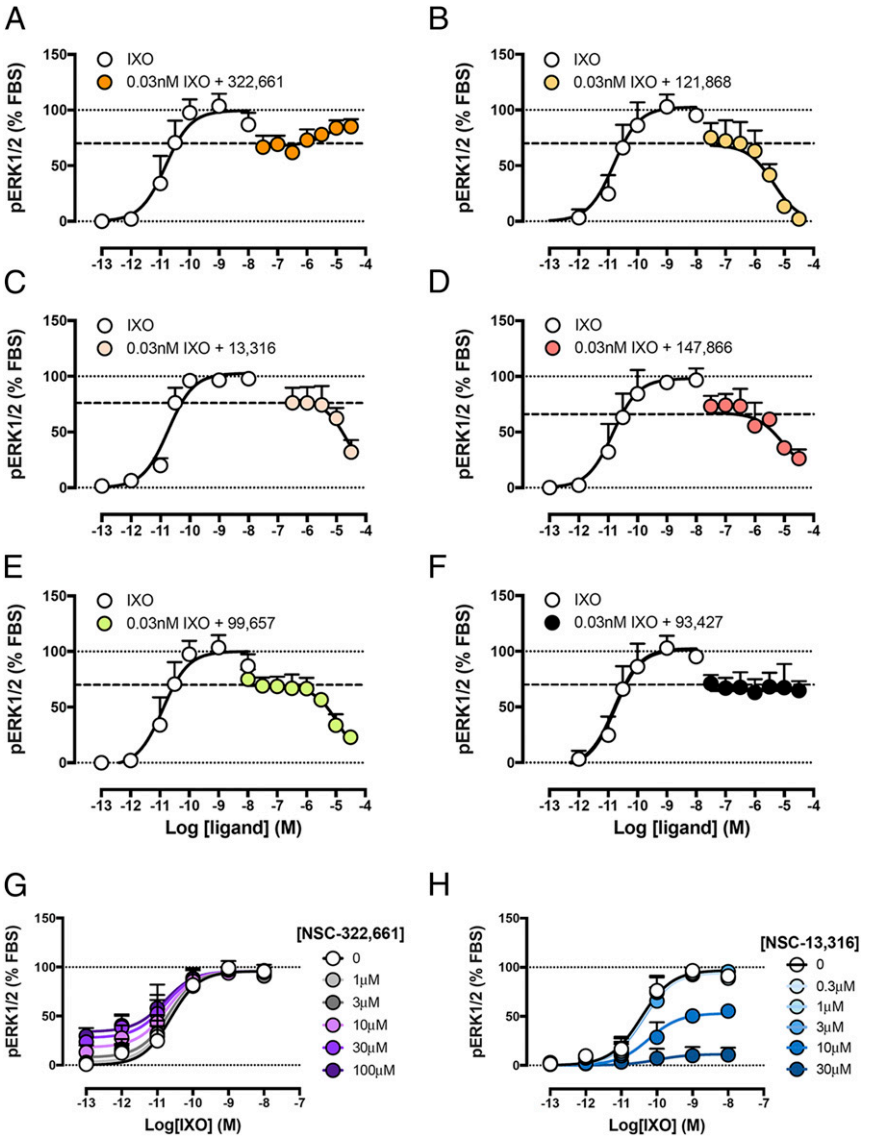

Fig. 4. Functional signaling effects of the six selected NCI compounds on agonist-mediated pERK1/2 responses at the M_2 mAChR. (*A*–*E*) Functional interactions between 0.03 nM IXO and increasing concentrations of four NCI compounds in a titration interaction format are shown as follows. (*A*) NSC-322661. (*B*) NSC-121868. (*C*) NSC-13316. (*D*) NSC-147866. (*E*) NSC-99657. (*F*) NSC-93427. (*G* and *H*) Functional interactions between IXO and increasing concentrations of NSC-322661 (*G*) and NSC-13316 (*H*) in a full interaction format, to validate the distinctive allosteric properties of the two selected NCI compounds.

M_3 mAChRs. With the same method as used for the M_2 mAChR, we determined the levels of pERK1/2 upon IXO addition in the presence of absence of each of the six NCI compounds tested previously at the M_3 (Fig. 6) and M_1 mAChRs (Fig. 7). The three cross-hit compounds, NSC-322661, -121868, and -13316, appeared to antagonize the agonist-mediated response of IXO for both receptors. Excitingly, the two NCI compounds that were selected based on either the receptor active state (NSC-147866) or the inactive state (NSC-99657) had no significant effect on IXO-mediated pERK1/2 levels at either the M_3 or the M_1 mAChR (Figs. 6 *C* and *D* and 7 *C* and *D*). After a one-way ANOVA statistical test, comparing the maximal responses of IXO in absence and presence of a 10 μM concentration of each NCI compound, these two NCI compounds showed negligible differences, similar to the negative control NSC-93427 that had no effect on the M_2 mAChR. According to ensemble docking calculations, NSC-147866 and -99657 prefer to bind the cleft formed between ECL2 and ECL3, which is significantly different from the three cross-hit compounds that are predicted to bind to approximately the center of the extracellular vestibule (Fig. 5 *C* and *D*). Notably, NSC-147866 interacts with Phe-181 in ECL2, and NSC-99657 forms interactions with Asn-$410^{6.58}$ and Ile-417 in ECL3. These residues exhibit great diversity across five subtypes of the mAChRs (19), and comparison of the X-ray structures of the M_2 and M_3 receptors showed significant differences in the ECL2–ECL3 cleft (17), which apparently contribute to binding selectivity of the NSC-147866 and -99657 compounds.

Discussion

mAChRs are involved in some of the most debilitating diseases, both centrally—such as Parkinson's disease, Alzheimer's disease, and schizophrenia—and peripherally, such as asthma and heart dysfunctions (40). Although, several orthosteric cholinergic drugs have made their way to the market, all of them exhibit side effects. For example, trihexyphenidyl, a muscarinic antagonist used in some cases for the treatment of Parkinson's disease, induces drowsiness, anxiety, and blurred vision, as well as tachycardia (41, 42). Such high levels of off-target effects are primarily due to the poor selectivity profile of trihexyphenidyl, antagonizing multiple

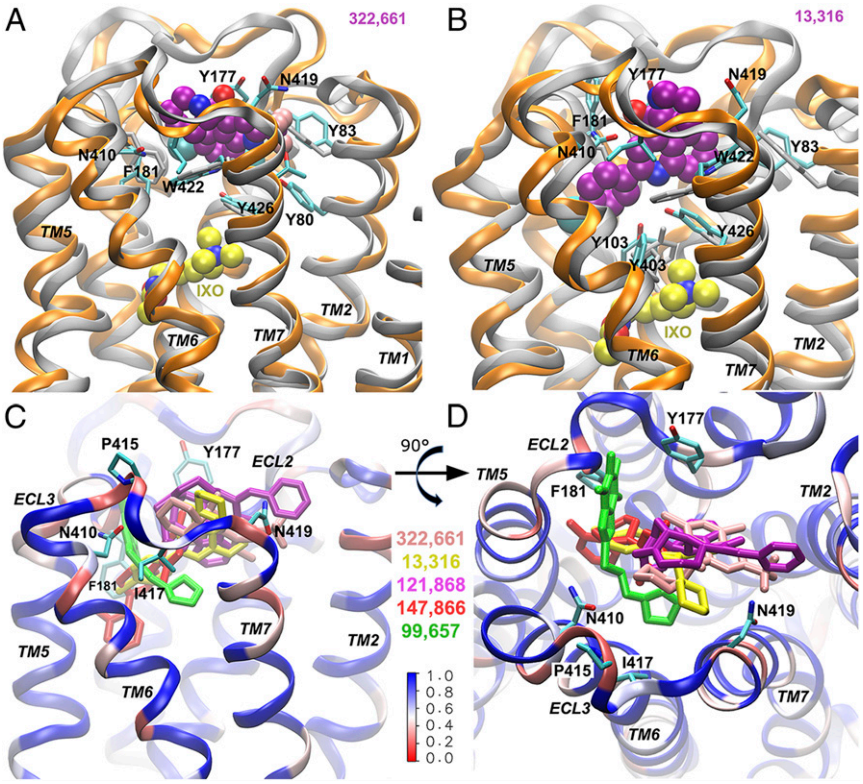

Fig. 5. The predicted most favorable binding poses of functional allosteric modulators of the M_2 mAChR obtained from ensemble docking calculations. (*A* and *B*) NSC-322661, a PAM that causes only slight conformational changes in the receptor (*A*) and NSC-13316, a NAM that binds deeper into the receptor and induces larger structural rearrangements of the TM helices with significant conformational changes in residues $Y426^{7.39}$, $W422^{7.35}$, $Y83^{2.64}$, and $F181^{ECL2}$ (*B*). The ligands are shown as spheres with carbons in yellow for IXO and purple for the allosteric modulators. The receptor is represented by orange ribbons, and residues found within 3 Å of the bound allosteric modulators are labeled and shown as sticks. The X-ray structure of the active M_2 mAChR (Protein Data Bank ID code 4MQS) is also shown in gray as reference. (*C* and *D*) Comparison of binding poses for the NSC-322661 (pink), NSC-13316 (yellow), NSC-121868 (purple), NSC-147866 (red), and NSC-99657 (green) compounds in the side (*C*) and extracellular (*D*) views. The compounds are shown as thick sticks and the interacting residues as thin sticks. The receptor is represented by ribbons colored by the sequence conservation across five subtypes of human mAChRs. Blue means high conservation 1, and red means low conservation 0.

mAChR subtypes simultaneously. This lack of selectivity from orthosteric site-targeting drugs is the consequence of a high degree of conservation of sequences and structures between each member of the mAChR family. It is thus not surprising that GPCR-based drug discovery, particularly for the mAChR family, has been recently shifting focus toward possibly less conserved and potentially more selective regions of the receptors, such as allosteric sites. Like most GPCRs, allosteric sites have been identified for the mAChRs; for these receptors, these sites are located predominantly within the extracellular loops and the top of the transmembrane domains. To date, the majority of allosteric ligands that have been identified for the mAChRs have come out of high-throughput screening programs and are lacking chemical diversity in their scaffolds. To address this issue, we have developed a computational-based method to efficiently identify novel allosteric scaffolds for the M_2 mAChR, with high potential for future development of more selective and more potent allosteric modulators. For instance, the M_2 mAChR plays a major role in modulating cardiac functions, whereby activation of this receptor typically results in a decrease in the heart rate and a reduction in the heart contraction forces. Therefore, selective drugs that could either enhance or inhibit the M_2 mAChR may be beneficial for treating heart diseases involving abnormal heart rate and heart failure (43). Through iterative computational modeling and experimental testing, here we report a successful structure-based approach for discovering chemically diverse allosteric modulators of the M_2 mAChR. We have combined aMD enhanced sampling simulations with *Glide* IFD to fully account for flexibility of the receptor in both the backbone and side chains. Experimental assays, including radioligand kinetic dissociation, equilibrium competition binding experiments, and functional assays, were used to test the computationally selected lead compounds and highlight their distinct allosteric properties as either PAMs or NAMs, depending on the orthosteric ligand used as probe.

Computationally, the Glide IFD method provided much improved docking compared with the Glide VSW. By using Glide IFD combined with aMD simulations for ensemble docking, 12 of the 38 computationally selected compounds were confirmed as allosteric ligands of the M_2 mAChR, with ∼3–30 μM (∼5.6–8.5 kcal/mol) binding affinity (Table 1 and Fig. 2*B*), confirming the critical importance of incorporating receptor flexibility into GPCR drug design. For instance, by using only the X-ray crystal structures for virtual screening, it appears that ∼50–60% of the experimentally confirmed NCI ligands of the M_2 mAChR would have been missed. Furthermore, the rmse values between docking and experimental binding energies were ∼4–5 kcal/mol, although these differences were significantly reduced, to 2.1 kcal/mol where BE_{avg} was used for docking against the active M_2 receptor. Experimentally, we successfully validated 19 NCI compounds as allosteric modulators of the M_2 mAChR, with 12 with affinity ≤30 μM. Additionally, of the 19 NCI compounds that did not significantly alter the dissociation rate of [^{3}H]NMS, and were therefore classified as "nonallosteric ligands," none of them appeared to affect the specific equilibrium binding of [^{3}H]NMS, suggesting that these ligands were simply not binders of the M_2

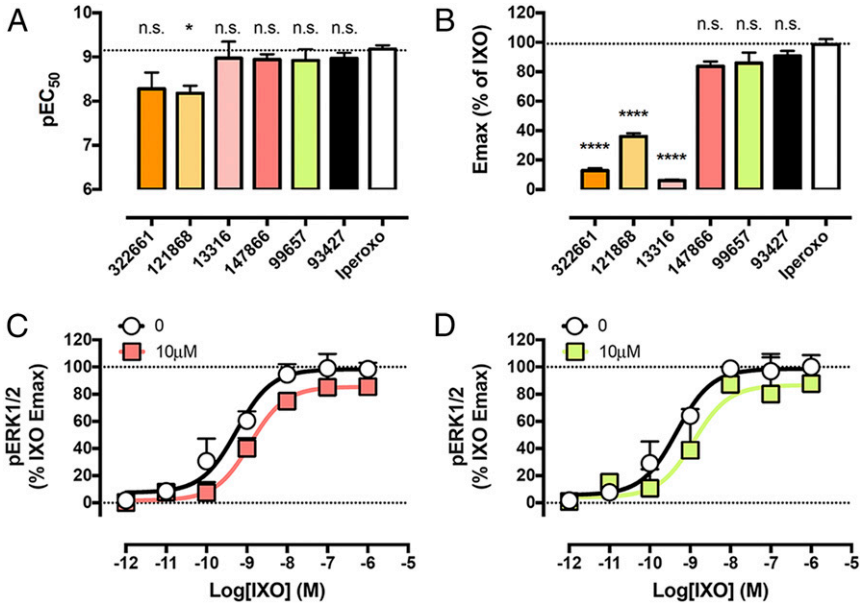

Fig. 6. Functional signaling effects of the six selected NCI compounds on agonist-mediated pERK1/2 responses at the M_3 mAChR. (*A* and *B*) Effect of 10 μM concentration of each NCI compound on IXO potency (*A*) and IXO maximal response (*B*). (*C* and *D*) Full interaction curves between IXO and NSC-147866 (*C*) or NSC-99657 (*D*) at a concentration of 10 μM. Statistical analyses were performed by one-way ANOVA between the control value, IXO potency, or Emax, using Prism (Version 7.01), and statistical significance was taken as $P < 0.05$.

mAChR, as opposed to potential competitive ligands. Further validating our method, the NCI compounds that share structural similarities with already known modulators (e.g., the strychnine-like NSC-121868) did come back as allosteric ligands in our experimental testing. Specifically, when investigating the effect of strychnine on the M_2 mAChR, we confirmed that the modulator was able to bind to the allosteric site with an affinity close to micromolar, $pK_B = 5.78 \pm 0.04$, and exhibit positive cooperativity with the radioligand [^{3}H]NMS, $\text{Log}\alpha_{NMS} = 0.21 \pm 0.06$ (*SI Appendix*, Fig. S4*C*), confirming previous findings (44). Similarly, the binding affinity of NSC-121868 was very close to that of strychnine (*SI Appendix*, Fig. S4*D*). In contrast, we identified negative cooperativity between NSC-121868 and [^{3}H]NMS, suggesting that the small structural changes between strychnine and NSC-121868 (i.e., stereospecificity of a central carbon in the core and addition of a phenylethene group) had no effect on the binding affinity, but rather appeared to switch the ligand from PAM to NAM for antagonist binding. Among

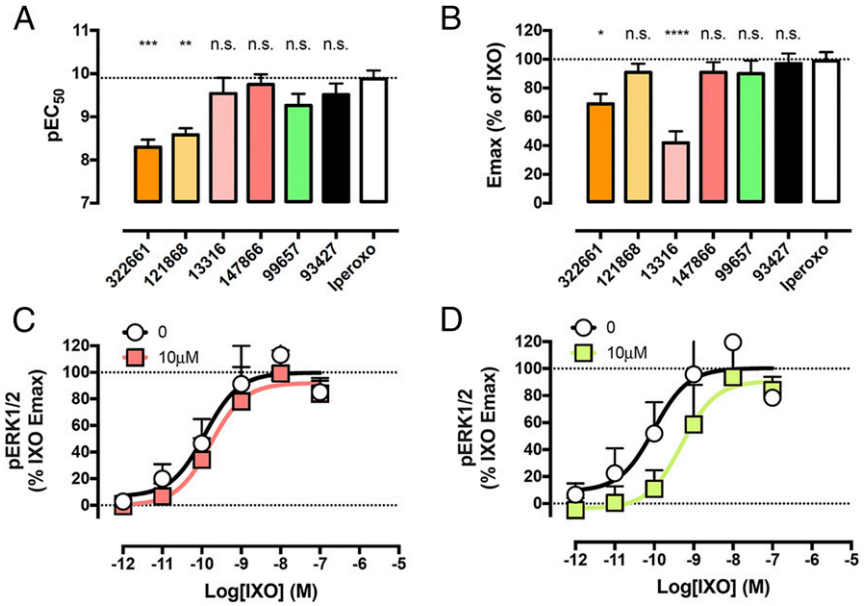

Fig. 7. Functional signaling effects of the six selected NCI compounds on agonist-mediated pERK1/2 responses at the M_1 mAChR. (*A* and *B*) Effect of 10 μM concentration of each NCI compounds on IXO potency (*A*), and IXO maximal response (*B*). (*C* and *D*) Full interaction curves between IXO and NSC-147866 (*C*) or NSC-99657 (*D*) at 10 μM. Statistical analyses were performed by one-way ANOVA between the control value, IXO potency or Emax, using Prism (Version 7.01), and statistical significance was taken as $P < 0.05$.

the seven computationally selected lead compounds that were predicted to bind both the active and inactive M_2 mAChR conformations, five of them indeed exhibited binding cooperativity with the antagonist [^{3}H]NMS (Fig. 2*C*) and/or the agonist IXO (Fig. 2*D*), whereas the remaining two (NSC-106464 and -177862) were not effective in slowing dissociation of the antagonist radioligand and are thus most likely nonbinders. From the 16 compounds that were predicted to predominantly bind the active conformation of M_2 mAChR, 3 of them (NSC-308814, -379697, and -147866) exhibited affinity at ∼10μM. Four of 15 compounds that were predicted to specifically bind the inactive conformation of the receptor were also confirmed as ∼30 μM binders. Thus, we can confirm that using our ensemble docking method, selecting compounds that were computationally binders of both active and inactive conformations of the receptor, we achieved an outstanding 70% success rate in identifying allosteric ligands. In comparison, by using either the active state or the inactive state X-ray conformations, the success rate of identifying allosteric modulators was reduced to ∼20–25%.

Importantly, substantial chemical diversity was found among the NCI compounds that bind allosterically to the M_2 mAChR (Fig. 3). Within the subset of five ligands selected based on both active and inactive receptor conformations, only NSC-322661 and -13316 showed some chemical identity, both quinolone-based ligands, which is a scaffold that has been shown to bind and antagonize the muscarinic receptors, such as NSC-23766 (45). Additionally, NSC-143491 is an anthraquinone-based ligand. Anthracycline ligands have been shown to be highly effective anticancer drugs, although they are also well known for their deleterious cardiotoxicity side effects (46). Indeed, mitoxantrone was shown to bind to muscarinic receptors in isolated heart muscles of guinea pigs, and potentially in an allosteric manner, because the inhibition binding curve of mitoxantrone appeared incomplete against the antagonist radioligand, [^{3}H]QNB (47). Another anthraquinone, doxorubicin, has been shown to reduce the maximal negative ionotropic effects of carbachol in isolated guinea pig hearts (48), consistent with an antagonist effect on the muscarinic system in this rodent. In summary, most of the NCI compounds that we identified as allosteric modulators are small organic molecules, containing several heteroatoms. They could easily be chemically modified, and therefore have great potential to pave the way for lead optimization to design more potent allosteric modulators of the M_2 mAChR. Excitingly, of the selected five NCI compounds that interacted allosterically at the M_2 mAChR with IXO, two of them (NSC-147866 and -99657) showed no effect on the agonist-mediated pERK1/2 responses at the M_3 subtype. Ensemble docking calculations showed that, unlike the three cross-hit compounds, which bind similarly to the center of the extracellular vestibule in both the active and inactive states of the M_2 mAChR, NSC-147866 and -99657 prefer to bind the cleft formed between ECL2 and ECL3. The ECL2– ECL3 cleft showed significant differences in the M_2 and M_3 X-ray structures (17) and involved diverse residues across different subtypes of the mAChRs (19). These differences likely contribute to binding selectivity of the two selected NCI compounds.

Conclusions

In this study, we examined the applicability of aMD enhanced sampling simulations and receptor ensemble docking in characterization of the receptor flexibility and successful design of GPCR allosteric modulators. Using the rather small NCI chemical database (∼1,600 compounds), we developed a successful method of identification of chemically diverse allosteric modulators of the M_2 mAChR. These ligands are mostly small organic molecules and show potential for structure–activity relationship studies to develop more potent allosteric modulators. This work will set the stage for future lead optimization efforts that combine computational free energy calculations and synthetic biochemical experiments. It will be important to examine the selectivity of these chemically diverse allosteric modulators on the M_2 receptor vs. other subtypes of mAChRs. This work can also provide useful guidance for future drug design efforts using larger chemical databases [e.g., ZINC (49) and ChemBridge (50)], targeting allosteric sites of the M_2 receptor and other medically important GPCRs.

Methods

aMD simulations were carried out on both the inactive QNB(antagonist)-bound and active IXO(agonist)-nanobody-bound M_2 mAChR (*SI Appendix*, Fig. S1). Structural clustering of the simulation snapshots was carried out to construct representative receptor ensembles that account for the receptor flexibility. In the first round, 10 top-ranked compounds were selected from *Glide* VSW calculations for experimental testing. Although one of these compounds significantly slowed down dissociation of the antagonist radioligand, [^{3}H]NMS, which is a hallmark of the allosteric mode of action, none of them exhibited high affinity in the binding assays. In the second round, retrospective docking of known ligands, including antagonists, agonists, and allosteric modulators, showed that *Glide* HTVS+IFD provided much improved docking enrichment factors compared with the VSW. It was thus applied for prospective docking of chemical compounds obtained from the NCI chemical database to select 38 new top-ranked compounds for experimental testing. From this second set, 19 NCI compounds that significantly slowed the dissociation rate of the antagonist radioligand were selected for further radioligand binding experiments, including a direct two-way equilibrium competition binding with [^{3}H]NMS, to obtain both binding affinity, pK_B, and cooperativity factor, $\text{Log}\alpha_{NMS}$, as well as a three-way equilibrium competition binding with [^{3}H]NMS and the agonist, IXO, allowing us to estimate the cooperativity factor for the agonist, $\text{Log}\alpha_{IXO}$. Finally, four NCI compounds were investigated thoroughly regarding their functional allosteric signaling effects on the agonist-induced pERK1/2 responses. Details of the computational aMD simulations and docking protocols, experimental binding and functional assays, and analysis methods are provided in *SI Appendix*.

ACKNOWLEDGMENTS. We thank Lei Huang (University of Chicago) for assistance with calculating the GAAMP ligand force field parameters and Thijs Beuming (Schrödinger, Inc.) for help with part of the virtual screening calculations. Computing time was provided on the Gordon and Stampede supercomputers through Extreme Science and Engineering Discovery Environment awards TG-MCA93S013 and TG-MCB140011 and the Hopper and Edison supercomputers through National Energy Research Scientific Computing Center Project M1395. This work was supported by National Science Foundation Grant MCB1020765; NIH Grant GM31749; the Howard Hughes Medical Institute, and the National Biomedical Computation Resource. This work was also supported by National Health and Medical Research Council of Australia (NHMRC) Program Grants 519461 and APP1055134 and Project Grant APP1082318. C.V. is an Australian Research Council Future Fellow. A.C is a Senior Principal Research Fellow and P.M.S is a Principal Research Fellow of the NHMRC.

1. Overington JP, Al-Lazikani B, Hopkins AL (2006) How many drug targets are there? *Nat Rev Drug Discov* 5(12):993–996.
2. Neubig RR, Spedding M, Kenakin T, Christopoulos A; International Union of Pharmacology Committee on Receptor Nomenclature and Drug Classification (2003) International Union of Pharmacology Committee on Receptor Nomenclature and Drug Classification. XXXVIII. Update on terms and symbols in quantitative pharmacology. *Pharmacol Rev* 55(4):597–606.
3. Christopoulos A (2002) Allosteric binding sites on cell-surface receptors: Novel targets for drug discovery. *Nat Rev Drug Discov* 1(3):198–210.
4. Shoichet BK, Kobilka BK (2012) Structure-based drug screening for G-protein-coupled receptors. *Trends Pharmacol Sci* 33(5):268–272.
5. Weiss DR, et al. (2013) Conformation guides molecular efficacy in docking screens of activated β-2 adrenergic G protein coupled receptor. *ACS Chem Biol* 8(5):1018–1026.
6. Kruse AC, et al. (2013) Muscarinic receptors as model targets and antitargets for structure-based ligand discovery. *Mol Pharmacol* 84(4):528–540.
7. Booth B, Zemmel R (2004) Prospects for productivity. *Nat Rev Drug Discov* 3(5):451–456.
8. Allen JA, Roth BL (2011) Strategies to discover unexpected targets for drugs active at G protein-coupled receptors. *Annu Rev Pharmacol Toxicol* 51:117–144.
9. Caulfield MP, Birdsall NJ (1998) International Union of Pharmacology. XVII. Classification of muscarinic acetylcholine receptors. *Pharmacol Rev* 50(2):279–290.
10. Ivetac A, McCammon JA (2012) A molecular dynamics ensemble-based approach for the mapping of druggable binding sites. *Methods Mol Biol* 819:3–12.
11. Miao Y, Nichols SE, McCammon JA (2014) Mapping of allosteric druggable sites in activation-associated conformers of the M2 muscarinic receptor. *Chem Biol Drug Des* 83(2):237–246.
12. Christopoulos A (2014) Advances in G protein-coupled receptor allostery: From function to structure. *Mol Pharmacol* 86(5):463–478.

13. Christopoulos A, Kenakin T (2002) G protein-coupled receptor allosterism and complexing. *Pharmacol Rev* 54(2):323–374.
14. Wootten D, Christopoulos A, Sexton PM (2013) Emerging paradigms in GPCR allostery: Implications for drug discovery. *Nat Rev Drug Discov* 12(8):630–644.
15. Conn PJ, Christopoulos A, Lindsley CW (2009) Allosteric modulators of GPCRs: A novel approach for the treatment of CNS disorders. *Nat Rev Drug Discov* 8(1):41–54.
16. Haga K, et al. (2012) Structure of the human M2 muscarinic acetylcholine receptor bound to an antagonist. *Nature* 482(7386):547–551.
17. Kruse AC, et al. (2012) Structure and dynamics of the M3 muscarinic acetylcholine receptor. *Nature* 482(7386):552–556.
18. Kruse AC, et al. (2013) Activation and allosteric modulation of a muscarinic acetylcholine receptor. *Nature* 504(7478):101–106.
19. Thal DM, et al. (2016) Crystal structures of the M1 and M4 muscarinic acetylcholine receptors. *Nature* 531(7594):335–340.
20. Dror RO, et al. (2011) Activation mechanism of the β2-adrenergic receptor. *Proc Natl Acad Sci USA* 108(46):18684–18689.
21. Niesen MJM, Bhattacharya S, Vaidehi N (2011) The role of conformational ensembles in ligand recognition in G-protein coupled receptors. *J Am Chem Soc* 133(33): 13197–13204.
22. Provasi D, Artacho MC, Negri A, Mobarec JC, Filizola M (2011) Ligand-induced modulation of the free-energy landscape of G protein-coupled receptors explored by adaptive biasing techniques. *PLOS Comput Biol* 7(10):e1002193.
23. Kohlhoff KJ, et al. (2014) Cloud-based simulations on Google Exacycle reveal ligand modulation of GPCR activation pathways. *Nat Chem* 6(1):15–21.
24. Shan J, Khelashvili G, Mondal S, Mehler EL, Weinstein H (2012) Ligand-dependent conformations and dynamics of the serotonin 5-HT(2A) receptor determine its activation and membrane-driven oligomerization properties. *PLOS Comput Biol* 8(4): e1002473.
25. Grossfield A (2011) Recent progress in the study of G protein-coupled receptors with molecular dynamics computer simulations. *Biochim Biophys Acta* 1808(7):1868–1878.
26. Johnston JM, Filizola M (2011) Showcasing modern molecular dynamics simulations of membrane proteins through G protein-coupled receptors. *Curr Opin Struct Biol* 21(4): 552–558.
27. Vanni S, Rothlisberger U (2012) A closer look into G protein coupled receptor activation: X-ray crystallography and long-scale molecular dynamics simulations. *Curr Med Chem* 19(8):1135–1145.
28. Li J, Jonsson AL, Beuming T, Shelley JC, Voth GA (2013) Ligand-dependent activation and deactivation of the human adenosine A(2A) receptor. *J Am Chem Soc* 135(23): 8749–8759.
29. Dror RO, et al. (2011) Pathway and mechanism of drug binding to G-protein-coupled receptors. *Proc Natl Acad Sci USA* 108(32):13118–13123.
30. Dror RO, et al. (2013) Structural basis for modulation of a G-protein-coupled receptor by allosteric drugs. *Nature* 503(7475):295–299.
31. Miao Y, Nichols SE, Gasper PM, Metzger VT, McCammon JA (2013) Activation and dynamic network of the M2 muscarinic receptor. *Proc Natl Acad Sci USA* 110(27): 10982–10987.
32. Miao Y, Caliman AD, McCammon JA (2015) Allosteric effects of sodium ion binding on activation of the m3 muscarinic G-protein-coupled receptor. *Biophys J* 108(7): 1796–1806.
33. Miao Y, Nichols SE, McCammon JA (2014) Free energy landscape of G-protein coupled receptors, explored by accelerated molecular dynamics. *Phys Chem Chem Phys* 16(14): 6398–6406.
34. Lin J-H, Perryman AL, Schames JR, McCammon JA (2002) Computational drug design accommodating receptor flexibility: The relaxed complex scheme. *J Am Chem Soc* 124(20):5632–5633.
35. Amaro RE, Baron R, McCammon JA (2008) An improved relaxed complex scheme for receptor flexibility in computer-aided drug design. *J Comput Aided Mol Des* 22(9): 693–705.
36. Shi LM, et al. (2000) Mining and visualizing large anticancer drug discovery databases. *J Chem Inf Comput Sci* 40(2):367–379.
37. Granier S, Kobilka B (2012) A new era of GPCR structural and chemical biology. *Nat Chem Biol* 8(8):670–673.
38. Vogel WK, Sheehan DM, Schimerlik MI (1997) Site-directed mutagenesis on the m2 muscarinic acetylcholine receptor: The significance of Tyr403 in the binding of agonists and functional coupling. *Mol Pharmacol* 52(6):1087–1094.
39. Valant C, Felder CC, Sexton PM, Christopoulos A (2012) Probe dependence in the allosteric modulation of a G protein-coupled receptor: Implications for detection and validation of allosteric ligand effects. *Mol Pharmacol* 81(1):41–52.
40. Kruse AC, et al. (2014) Muscarinic acetylcholine receptors: Novel opportunities for drug development. *Nat Rev Drug Discov* 13(7):549–560.
41. Blumensohn R, Razoni G, Shalev A, Munitz H (1986) Bradycardia due to trihexyphenidyl hydrochloride. *Drug Intell Clin Pharm* 20(10):786–787.
42. Friedman Z, Neumann E (1972) Benzhexol-induced blindness in Parkinson's disease. *BMJ* 1(5800):605.
43. Harvey RD (2012) Muscarinic receptor agonists and antagonists: Effects on cardiovascular function. *Handbook Exp Pharmacol* 208(208):299–316.
44. Lazareno S, Birdsall NJ (1995) Detection, quantitation, and verification of allosteric interactions of agents with labeled and unlabeled ligands at G protein-coupled receptors: Interactions of strychnine and acetylcholine at muscarinic receptors. *Mol Pharmacol* 48(2):362–378.
45. Levay M, et al. (2013) NSC23766, a widely used inhibitor of Rac1 activation, additionally acts as a competitive antagonist at muscarinic acetylcholine receptors. *J Pharmacol Exp Ther* 347(1):69–79.
46. Geisberg CA, Sawyer DB (2010) Mechanisms of anthracycline cardiotoxicity and strategies to decrease cardiac damage. *Curr Hypertens Rep* 12(6):404–410.
47. Chugun A, et al. (2000) Anti-muscarinic actions of mitoxantrone in isolated heart muscles of guinea pigs. *Eur J Pharmacol* 407(1-2):183–189.
48. Chugun A, et al. (2001) Doxorubicin affects the cardiac muscarinic system in the rat. *J Vet Med Sci* 63(12):1315–1322.
49. Irwin JJ, Sterling T, Mysinger MM, Bolstad ES, Coleman RG (2012) ZINC: A free tool to discover chemistry for biology. *J Chem Inf Model* 52(7):1757–1768.
50. Groom CR, Bruno IJ, Lightfoot MP, Ward SC (2016) The Cambridge Structural Database. *Acta Crystallogr B Struct Sci Cryst Eng Mater* 72(Pt 2):171–179.